Synergetic effects of NH_3 and NO_X on the production and optical absorption of secondary organic aerosol formation from toluene photooxidation

Shijie Liu [a], Dandan Huang [b], Yiqian Wang [a], Si Zhang [a], Xiaodi Liu [a], Can Wu [a], Wei Du [a], Gehui Wang [a,c,*]

[a] Key Lab of Geographic Information Science of the Ministry of Education, School of Geographic Sciences, East China Normal University, Shanghai 210062, China

[b] State Environmental Protection Key Laboratory of Formation and Prevention of the Urban Air Pollution Complex, Shanghai Academy of Environmental Sciences, Shanghai 200233, China

[c] Institute of Eco-Chongming, Cuiniao Road, Chengjia Zheng, Shanghai 202150, China.

Corresponding author: Prof. Gehui Wang, e-mail: ghwang@geo.ecnu.edu.cn

Abstract

NH_3 is the most important alkaline gas in the atmosphere and one of the key species affecting the behaviors of atmospheric aerosols. However, the impact of NH_3 on secondary organic aerosol (SOA) formation remains poorly understood, especially the dynamic evolution of chemical compositions in the SOA formation process. In this study, a series of chamber experiments were performed to probe the individual and common effects of NH_3 and NO_X on toluene SOA formation through OH-photooxidation. The chemical compositions of toluene SOA were characterized using the Aerodyne high-resolution time-of-flight aerosol mass spectrometer (AMS). The SOA yield increased from 28.1% in the absence of NH_3 to 34.7% in the presence of NH_3 but decreased to 19.5% in the presence of NO_X. However, the highest SOA yield of 42.7% and the lowest carbon oxidation state (OS_C) occurred in the presence of both NH_3 and NO_X, indicating that the higher volatility products that formed in the presence of NO_X could partition into the particle-phase when NH_3 was added. This resulted in a synergetic effect on SOA formation when NH_3 and NO_X co-existed. The heterogeneous reaction was the main pathway by which NH_3 participated in SOA formation in the photooxidation process. The synergetic effect of NH_3 and NO_X was also observed in SOA optical absorption. A peak at 280 nm, which is characteristic of organonitrogen imidazole compounds, was observed in the presence of NH_3 and its intensity increased when NO_X was added into the chamber. This work improves our understanding of how the synergistic interactions between NH_3 and NO_X influence SOA formation and offers new insights into mitigating haze pollution.

Keywords: Photooxidation; Toluene; NH_3; Dynamic characteristics; Synergistic effects

1 Introduction

Secondary organic aerosols (SOA) are an important component of atmospheric particulate matter (Moise et al., 2015;Liu et al., 2017), and can significantly affect atmospheric visibility, air quality, and human health (Paciga et al., 2014;Yang et al., 2016;Liu et al., 2017). Optical properties of SOA have been directly and indirectly linked to their effects on the climate (Laskin et al., 2015;Xie et al., 2017;Peng et al., 2020). Because of the complexity of their chemical components, oxidation processes, and environmental factors, SOA formation mechanisms are very complex and the current understanding of SOA formation is incomplete. This limited understanding hampers the ability of models to predict the magnitudes, dynamics, and distributions of atmospheric aerosols from particulate and precursor emissions (Ortiz-Montalvo et al., 2014). In the past decades, although our understanding of SOA formation mechanisms has been constantly improving, there is still a gap between the simulated SOA concentration in large-scale atmospheric models and field observations (Volkamer et al., 2006;Yang et al., 2018).

Ammonia (NH_3) is the most abundant and ubiquitous alkaline inorganic gas in the atmosphere and one of the critical factors influencing SOA formation (Wang et al., 2016;Wang et al., 2018b;Chen et al., 2019). Some studies have noted that the presence of NH_3 can contribute to the formation of more aerosol mass through photooxidation (Na et al., 2007;Li et al., 2018). Na et al. (2007) observed that aerosol yields in the α-pinene-ozone oxidation system increased by 8% when NH_3 was added. Li et al. (2018) reported that the presence of NH_3 in the aromatic hydrocarbon photooxidation system

increased aerosol size growth potentials (by 7%–108%), and resulted in enhanced SOA formation. Qi et al. (2020) found that the concentration and average diameter of SOA showed an immediate and rapid increase after adding NH_3. Furthermore, the acid-base reactions between NH_3/NH_4^+ and the carboxyl groups in SOA molecules might enhance SOA formation (Qi et al., 2020;Liu et al., 2015). The condensable ammonium salts formed from the reaction between NH_3 and organic acids reduce the volatility of the organic acids by several orders of magnitude (Paciga et al., 2014), and act as particle-phase organics that further promote SOA formation (Na et al., 2007;Huang et al., 2012;Chen et al., 2019;Qi et al., 2020;Wu et al., 2020). In addition, carbonyls can undergo nucleophilic attack by NH_3 through the Maillard reactions and form the corresponding iminium intermediates (Noziere et al., 2009;Laskin et al., 2015;Liu et al., 2015). The iminium intermediates can continue to react with carbonyls, which activates further transformations such as the formation of heterocyclic compounds and oligomerization reactions and forms condensation (oligomeric) products with more stable secondary imines (Schiff bases) (Laskin et al., 2014). Both Noziere et al. (2009) and Ortiz-Montalvo et al. (2014) reported NH_3 is an efficient catalyst for reactions with carbonyl compounds to form nitrogen-containing organic aerosols (NOA). The reaction between carbonyl and NH_3 can significantly decrease the volatility of oxidation products, which further increases the yield of SOA (Lee et al., 2013;Zhang et al., 2015a;Qi et al., 2020). Babar et al. (2017) found that the substantial formation of secondary imines in the presence of NH_3 was responsible for the higher α-pinene SOA yields. However, not all studies have shown that the presence of NH_3 increases SOA

yields. One study observed that NH_3 suppressed SOA formation under certain ozonation conditions (Ma et al., 2018b). Furthermore, the consumption of NH_3 by Criegee intermediates was reported to decrease the secondary ozonide yield and thus affect SOA formation.

Nitrogen oxides (NO_X = NO + NO_2), which are mainly emitted from the combustion of fossil-fuels, have received significant attention due to their effects on the photooxidation process of volatile organic compounds (VOCs) and SOA formation (Surratt et al., 2006;Ng et al., 2007b;Draper et al., 2015;Berkemeier et al., 2016;Sarrafzadeh et al., 2016;Zhao et al., 2018). A clear increase at first and then a decrease in the SOA yield was found with increasing NO_X concentration from the laboratory experiments with both anthropogenic (trimethylbenzene) and biogenic (β-pinene) VOCs (Sarrafzadeh et al., 2016;Yang et al., 2020). The competitive chemistry of organic peroxyl radicals (RO_2) with hydroperoxyl radicals (HO_2) and NO was responsible for the variability in SOA formation (Ng et al., 2007a;Xu et al., 2014;Jiang et al., 2020). RO_2 mainly reacts with HO_2 under low-NO_X conditions to form oxidation products with lower volatility, which may enable it to partition into the particle-phase and contribute to the SOA mass (Ng et al., 2007a). While the RO_2 + NO reaction is dominant in high-NO_X conditions, the increase in volatile products formed through fragmentation was responsible for the decrease in SOA yield with increasing NO_X (Zhao et al., 2018;Liu et al., 2019a;Xu et al., 2020). In addition, the increase of OH concentration formed through NO + HO_2 →NO_2 + OH reaction at low-NO_X conditions, and a suppressing effect of NO_X on OH formation under high-NO_X conditions was

partly responsible for the first increasing and then decreasing trend of SOA yield with NO_X concentration (Sarrafzadeh et al., 2016;Bates et al., 2021).

In the last decade, atmospheric pollutants in China have changed significantly in their concentrations and composition (Wang et al., 2015;Xia et al., 2016) with the emissions of SO_2 and NO_X decreased by 75% from 2007–2015 and 10% from 2011–2015, respectively (de Foy et al., 2016;Vu et al., 2019;Wang et al., 2020). However, owing to the lack of regulation regarding NH_3 emissions, NH_3 emissions increased by ~30 % from 2008–2016 over the North China Plain (Liu et al., 2018). As has been pointed out in previous research, the promoting effect of NH_3 on the formation of SOA may counteract the decreases in aerosol formation due to reductions in SO_2 and NO_X (Zhang et al., 2021a). Indeed, field observation and model simulation have pointed out that the simultaneous control of NH_3 emissions in conjunction with SO_2 emission is more effective in reducing $PM_{2.5}$ than the process without NH_3 emissions control, and $PM_{2.5}$ concentration can be more effectively reduced if NH_3 emission is decreased as much as that of SO_2 (Erisman and Schaap, 2004). Hence, the mechanism by which NH_3 affects SOA formation has attracted more and more attention (Wang et al., 2018a;Ge et al., 2019;Zhang et al., 2021b). However, previous studies have not paid sufficient attention to the joint impacts of NH_3 and NO_X on the formation of SOA and its corresponding optical properties. Due to the lack of real time detection methods for SOA chemical composition, the dynamic characteristics of how NH_3 participates in SOA formation via photooxidation have not been extensively studied.

Toluene is one of the most abundant aromatic VOCs in the urban atmosphere,

which is also an important source of brown carbon (Laskin et al., 2010;Ma et al., 2018a). The effects of NH_3 and NO_X on SOA formation through the toluene photooxidation process were investigated in this study. The chemical composition of toluene SOA was characterized on-line with an aerosol mass spectrometer and the characteristics of SOA chemical composition under different conditions were further explored by applying a positive matrix factorization (PMF) analysis. The optical properties of toluene SOA particles were determined based on a UV-vis spectrum analysis. Possible mechanisms of the effects of both NH_3 and NO_X on SOA formation were discussed. The results will help us to better understand SOA formation mechanisms under complex pollution conditions with elevated NH_3 and NO_X concentrations in an urban atmospheric environment.

2 Materials and Methods

2.1 Photooxidation chamber experiments

All toluene photooxidation experiments were performed in a 4 m^3 chamber. The chamber has been described in detail in our previous study (Liu et al., 2021). Briefly, the chamber was constructed with a 0.08 mm-thick FEP-Teflon film. 50 UV-B lamps (TUV36W, Philips) with peak wavelengths of 254 nm were set up around the chamber and used as the light source to drive OH radical formation through hydrogen peroxide (H_2O_2) photolysis. Mirror surfaced stainless steel was used as the interior wall of the enclosure to maximize and homogenize the interior light intensity. All experiments

were performed at room temperature (293~298 K) and atmospheric pressure was maintained in the chamber at all times.

Before each experiment, the chamber was flushed with zero air for at least 18 hours, after which the concentration of particles was less than 1 cm^{-3}. Zero air was generated by a zero air supply (111-D3N, Thermo Scientific^{TM}, USA). The flow rate of zero air was controlled at 20 L min^{-1} by a mass flow controller (D088C/ZM, Beijing Sevenstar Electron Corporation) during the process of chamber reaction bag inflating. The relative humidity (RH) of zero air was about 20%. For each experiment, measured amounts of toluene (Sigma-Aldrich, analytically pure) and H_2O_2 solution (Sigma-Aldrich, 30 wt% in H_2O) were injected into a Teflon bulb with micro syringes. Zero air was passed through the injection tube to make sure all the liquids had evaporated to the gas-phase and were blown into the chamber. Toluene concentration was measured with a Proton Transfer Reaction-Mass Spectrometry (PTR-ToF-MS, Ionicon Analytik, Austria). The evolution of toluene concentration for different experiments was shown in Fig. S1. The OH concentration in the chamber was calculated based on the first order decay of toluene concentration. There was no obvious difference of OH concentrations in the different NO_X and NH_3 levels (Fig. S2). The average OH concentration over the entire reaction period was 5.87×10^7 molecule cm^{-3}. NO_X (Air Liquid Shanghai, 510 ppm NO_2 in N_2) and/or NH_3 (Air Liquid Shanghai, 502 ppm NH_3 in N_2) were introduced directly into the chamber to reach the required concentrations. For experiments with NO_X, although only NO_2 was introduced into the chamber before photooxidation, NO could be formed through NO_2 photolysis under the UV light irradiation, so NO always

coexisted with NO_2 in the photooxidation system (Zhao et al., 2018). NOx concentration was measured online by the NO-NO_2-NOx analyzer (Model 42C, Thermo Electron Corporation, USA). Each experiment was performed without seed aerosols. After all the reactants were added, the chamber stood quietly for 10 min without turning on the light to ensure that the reactant gases in the chamber were evenly mixed. The photooxidation started when the UV light was turn on.

The experimental conditions for the toluene photooxidation are listed in Table 1. In our work, the OH and toluene concentrations were higher than those of urban conditions. The purpose of the high OH and toluene concentrations is to obtain enough particle production samples for off-line collections and accurate measurements. The toluene concentrations remained stable under the different experimental conditions, the variations of toluene-derived SOA mass concentration and yield were only affected by the different NO_2 and/or NH_3 concentrations in this study. Toluene was studied here as the representative of total aromatic VOCs in the urban atmosphere, thus its concentration used in this study was much higher than that in the real atmosphere. However, the concentration ratio of toluene to OH in this study is similar to that under the real atmospheric conditions (Prinn et al., 1995;Zou et al., 2015).

2.2 Particle concentration measurements

For each experiment, a scanning mobility particle sizer (SMPS) was used to record the particle size distribution and volume concentration of the toluene-derived SOA. The SMPS was composed of a differential mobility analyzer (DMA model 3081, TSI Inc.,

USA) and a condensation particle counter (CPC model 3776, TSI Inc., USA) which were used for screening particles with specific electrical mobility diameter (from 14.1 nm to 736.5 nm) and for counting the number of the selected particles, respectively. The sheath gas velocity was 3 L min^{-1} and the sample gas velocity was 0.3 L min^{-1}. The size scan was repeated every 5 min. During each scan circle, the scan time was 240 s, and the particle sizes ranged from 13.6 nm to 726.5 nm. A density of 1.4 g m^{-3}, which was measured by Ng et al. (2007), was used for the calculation of toluene SOA mass concentration from the particle volume concentration (Ng et al., 2007b).

2.3 Chemical characterization

In this study, the toluene SOA chemical compositions were characterized with an on-line high-resolution time-of-flight aerosol mass spectrometer (HR-ToF-AMS, Aerodyne Research Inc. USA). The sample flow passed through a Nafion dryer and the RH of the sample gas was reduced to below 20% before entering the AMS. In the injection port, an aerodynamic lens focused particles with a vacuum aerodynamic diameter below 1 μm into a narrow beam. Particles impacted a flash vaporizer (600°C) at the rear of the sizing region under high vacuum (~10^{-7} Torr) and were subsequently ionized by electron impact ionization (70 eV). Then, the positively charged ions entered the ToF section and were separated. V-mode (m/Δm = ~2000) was used in the AMS ToF section to achieve the high signal-to-noise ratio. The separated ion fragments were analyzed by a mass spectrometer with scans from 1 to 300 m/z. The composition-dependent collection efficiency (CE) was applied to the data based on the methods

established by Middlebrook et al. (2012). For mass concentration calculations, 1.1, 1.2, and 1.4 were applied as the default relative ionization efficiency (RIE) values of nitrate, sulfate, and organic compounds, respectively. The standard AMS data analysis software SQUIRREL 1.63B coupled with PIKA 1.23B in the Igor Pro (WaveMetrics, Inc., Portland, Oregon), which were retrieved from http://cires1.colorado.edu/jimenez-group/ToFAMSResources/ToFSoftware/, were used for the analysis of elemental ratios and the ion speciated compositions of toluene SOA in the chamber. Note that the elemental ratios (i.e., O/C, H/C, and N/C) and mass-to-carbon ratio (OM/OC) were all calculated using the Aiken-Ambient method for comparability with previous studies (Aiken et al., 2008). In order to further explore the changes in SOA chemical composition, a PMF of the high-resolution mass spectra was performed to determine the different organic aerosol (OA) factors during the toluene photooxidation process. We preformed the PMF analysis in the same way as Zhang et al. (2011), the details of which are provided in the Supporting Information.

2.4 Absorption measurements

The changes of absorption spectra and the absorbance of the toluene derived SOA under different conditions were determined using a UV spectrophotometer (UV-3600, Shimadzu, Japan) with a 1 cm cuvette. The SOA was collected from a 3 m^3 sample gas onto the 46.2 mm PTFE filter (Whatman™, UK). The collected SOA sample was dissolved in 5 mL of methanol (HPLC grade, > 99.8%) with 30 min of sonication. As reported by Chen and Bond (2010), > 92 % of SOA is extractable by organic solvents

(e.g., methanol), which means that almost all organic matter was extracted in this study. The filter extracts were filtered through 0.2 μm PTFE syringe filters to remove suspended insoluble particles. Before detection of the optical absorbance, a cuvette filled with pure methanol was scanned as a blank to provide a spectral background. The absorption was detected over the range of 200 to 800 nm with a resolution of 0.5 nm^{-1}. The light absorption coefficient of the particles at a specific wavelength λ (Abs_λ, M/m) was calculated according to Eq. R1:

$$Abs_\lambda=(A_\lambda-A_{700})\cdot\frac{V_l}{V_a\cdot L}\cdot\ln(10) \quad (R1)$$

where, A_{700} is the background value of light absorption intensity, calculated as the average value of light absorption intensity from 695–705 nm to reduce the limits of error in measurement; V_l and V_a are the volumes of methanol with dissolved particles and sampled air, respectively; and L is the optical path length. Because Abs_λ was strongly dependent on the amount of SOA, all Abs_λ results were normalized based on the SOA mass collected on the filter. The normalized result was defined as the mass absorption coefficient (MAC, $m^2\ g^{-1}$), calculated using Eq. R2:

$$MAC_\lambda=\frac{Abs_\lambda}{M} \quad (R2)$$

where, M ($\mu g\ m^{-3}$) represents the concentration of methanol-soluble organic carbon.

3 Result and Discussion

3.1 SOA formation

In order to investigate the effect of NH_3 and NO_X on SOA formation from toluene photooxidation, a control test was carried out. SOA yield (Y) is defined as Y =

259 $\Delta M_0/\Delta HC$, where ΔM_0 is the produced organic aerosol mass concentration (μg m^{-3}),
260 and ΔHC is the mass concentration of reacted toluene (μg m^{-3}). The evolution of SOA
261 mass concentrations and SOA yield at different conditions during the photooxidation
262 process were shown in Fig. 1. Recent experiments showed that the wall loss of organic
263 vapors to the Teflon walls should not be ignored (Zhang et al., 2014;Zhang et al.,
264 2015b), and represented a major challenge in investigating SOA formation with
265 environmental chambers (Krechmer et al., 2020). The formation of SOA in laboratory
266 chambers may be substantially suppressed due to losses of SOA-forming vapors to
267 chamber walls, but this effect on SOA formation have not yet been quantitatively
268 established. However, the particle wall loss rates were detected at the end of the
269 chamber experiment after the UV-lamps were turned off, and the mass concentration
270 was corrected with the same way of Jiang et al. (2020) and Pathak et al. (2007). After
271 the wall loss correction, the particle mass concentration was almost constant, the
272 different wall loss effect caused by gaseous oxidation products formed in the different
273 experiment conditions was considered remedied. ~~Interestingly, wall loss is increased~~
274 ~~66% and 205% in Exp.2 (in the presence of NH3) and Exp.3 (in the mixed condition of~~
275 ~~NH_3 and NO_X), respectively, when compared with the experiments with no NH_3 (Exp.1~~
276 ~~and 4). The larger particle wall loss in the presence of NH_3 could be explained by~~
277 ~~increasing condensation process of oxidized organic vapors onto the Teflon chamber~~
278 ~~wall via oligomerization (for dicarbonyls) and ionic dissociation/acid-base reaction (for~~
279 ~~organic acids).~~ There was a noticeable increase in the SOA mass concentration in the
280 presence of NH_3, which was consistent with previous studies (Qi et al., 2020;Chu et al.,

2016). The mass concentration of SOA increased from 637 ± 14.6 μg m^{-3} without NH_3 to a maximum of 867 ± 12.7 μg m^{-3} with 200 ppb NH_3. Previous studies attributed the enhancement of SOA to the formation of NOA from acid-base reactions between NH_3/NH_4^+ and carboxyl groups, or Maillard reactions of NH_3/NH_4^+ with carbonyl functional groups (Noziere et al., 2009;Ortiz-Montalvo et al., 2014;Liu et al., 2015;Qi et al., 2020). In contrast, SOA concentrations were lower in the presence of NO_X, and the maximum mass concentration of toluene SOA was only 452 ± 18.9 μg m^{-3} with 63 ppb initial NO_X. The branching of RO_2 loss among different pathways has an important influence on the product distribution and SOA formation. The fate of RO_2 mainly depends on the concentrations of NO_X (Zhao et al., 2018;Liu et al., 2019a;Xu et al., 2020). Several studies have shown that, instead of RO_2 reacting with RO_2/HO_2, NO would react with RO_2 to form the RO intermediate and produces more oxidation products with higher volatilities through fragmentation in the presence of NO_X (Zhao et al., 2018;Liu et al., 2019a;Xu et al., 2020). Highly volatile compounds cannot readily partition into the particle-phase, so this substantially suppresses the formation of SOA.

The NO_X and NH_3 had opposite effects on toluene SOA formation in this study. Interestingly, however, the highest SOA mass concentration (1020 ± 10.6 μg m^{-3}) occurred in the presence of both NO_X and NH_3, which was nearly 1.6 times higher than that observed in the absence of NO_X or NH_3. Although inorganic aerosol (i.e., NH_4NO_3) was formed from the interaction of NH_3 and NO_X in the chamber, the upper limit of the inorganic matter only accounted for 6.6% of the total mass of particulate matter (Table S1) in the NH_3 + NO_X experiment. Therefore, NH_4NO_3 was not the main cause of the

increase in particulate matter; the co-occurrence of NH_3 and NO_X had a synergistic effect on the SOA formation, because their combined effect on SOA formation was greater than the sum of their separate effects. Qi et al. (2020) found that the promotion of NH_3 on toluene SOA formation was more obviously under high NO_X concentration, SOA yield increased 3.7% and 4.6% for 70 ppb and 160 ppb initial NO_X concentration, respectively, when 200 ppb NH_3 was added into the chamber. Li et al. (2018) showed that the presence NH_3 can promote the particle size growth of SOA; at the same time, this particle growth rate was higher under low VOC/NO_X (or high NO_X) conditions. All in all, the joint effect of multiple environmental factors on SOA formation is not the simple summation of the influences of various factors on SOA formation. This may at least partly explain why predictions of SOA concentrations in large-scale atmospheric models, which typically describe SOA formation from data derived from chamber experiments, are frequently lower than field observations (Volkamer et al., 2006).

3.2 SOA chemical composition

The traditional SOA formation mechanism is based on the chemical compositions obtained through off-line detection of the chemical composition of SOA (Jang et al., 2002;Liu et al., 2019a;Xu et al., 2020). SOA is continually evolving in the atmosphere and the ageing process of SOA co-occurs with its formation process, resulting in the transformation of SOA chemical composition continuously proceeding during the photooxidation process~~, but little attention has been paid to the evolution of SOA chemical composition in previous studies~~. Therefore, the AMS was used for on-line

measurement of the SOA chemical composition and how the chemical composition evolved in the photooxidation process will be discussed in the following section.

Chemical composition of SOA is very complex. The average carbon oxidation state (OS_C) has been shown to be an ideal conceptual framework to describe changes in the degree of oxidation undergone by SOA (Kroll et al., 2011), and has been widely applied in field and laboratory studies (Chen et al., 2018;Mandariya et al., 2019). Average OS_C calculation was shown in Supporting Information. Fig. 2 shows the changes in the OS_C of toluene SOA formed in different experiments. Notably, toluene SOA OS_C values was in the range between -0.5 and 0, which is consistent with that of semi-volatile oxygenated organic aerosols (SV-OOA). However, the different OS_C values and the change trends observed for the toluene SOA formed in different conditions (with and without NH_3/NO_X) in Fig. 2 indicated that there was a photooxidation mechanism active during SOA formation, which ultimately changed the SOA chemical compositions.

The OS_C increased over time for all SOAs that were formed in the absence of NH_3. There are several possible reasons for the increasing trend of OS_C values. Firstly, a dynamic equilibrium of semi-volatile vapors may have been achieved between the particle-phase and gas-phase during the earlier toluene oxidation process. The increase of SOA led to a reduction in the concentration of gas-phase semi-volatile organic products. A decreasing concentration of gas-phase semi-volatile organic compound products would suppress their transformation from gas-phase to particulate-phase. More lower volatility gas-phase oxidation products with higher OS_C values would then

346 be shifted to the particle phase, which would be responsible for the continuing increase
347 of SOA and its OSc. Secondly, the formed SOA could have further been oxidized by
348 OH radical through heterogeneous reactions (Kourtchev et al., 2015;Liu et al., 2019b).
349 This could be the main reason for the increase in the OS_C when the SOA concentration
350 was no longer increasing. Finally, as pointed by Malecha and Nizkorodov (2016), even
351 if there was no OH radical in the chamber, the photodegradation of SOA can produce
352 small oxygenated volatile organic compounds (e.g. acetaldehyde OS_C=-1, and acetone
353 OS_C≈-1.3) under UV light irradiation. The photoproduction of OVOCs from SOA had
354 a lower OS_C value than that of SOA. Although the loss of SOA through
355 photodegradation is small, the OS_C value of SOA still had increased to a certain extent
356 (Malecha and Nizkorodov, 2016).

357 The fact that additional photochemical processing results in the dynamic evolution
358 of the OS_C over time has been demonstrated in both field and laboratory experiments
359 (Jimenez et al., 2009). The atmospheric oxidation of OA tends towards higher OS_C
360 regardless of the original OA source (Herndon et al., 2008). However, when NH_3 was
361 present, the OS_C of total SOA was almost unchanged for the whole photooxidation
362 period. Carboxyl and carbonyl are the main oxygen-containing functional groups
363 responsible for the toluene photooxidation production (Ji et al., 2017). An organic
364 ammonium salt with four H atoms can offset an increase in OS_C value caused by the
365 formation of organic acids/carboxy group with two O atoms through acid-base reactions
366 (Kuwata and Martin, 2012;Liu et al., 2015). In addition, NH_3/NH_4^+ may react with
367 carbonyl functional groups through Maillard reactions, consuming the oxygen atom in

368 the carbonyl group and leading to the formation of species with covalent carbon-
369 nitrogen bonds (Lee et al., 2013;Zhang et al., 2015a;Qi et al., 2020). Xu et al. (2018)
370 showed that imidazole compounds ($OS_C \approx -1.3$) generated through heterogeneous
371 reaction between NH_3 and carbonyl compounds might contribute to the decrease in the
372 OS_C of SOA. It is clear that an increase in OS_C caused by the formation of oxygen-
373 containing functional groups (e.g., carboxyl, carbonyl, etc.) would be counteracted
374 through acid-base reactions or Maillard reactions in the presence of NH_3. After 60 min
375 of UV light irradiation, there was no more SOA formation; however, the OS_C did
376 decrease slightly in Exp.2 and 3, illustrating that the NH_3 could continue to react with
377 SOA through heterogeneous processes. Huang et al. (2016) also pointed out that the
378 portion of semi-volatile products with low OS_C formed at the later stage of
379 photooxidation also contributed to the decreased OS_C.

380 The OS_C of the toluene SOA formed with NO_X was lower than that formed in the
381 absence of NO_X, no matter whether NH_3 was present in the chamber or not. This
382 indicated that an increased NO_X concentration benefits the formation of high volatility
383 oxidation products with lower OS_C values (Kroll et al., 2011;Jimenez et al., 2009).
384 However, the relationships between OS_C and SOA mass concentration with and without
385 NH_3 were the opposite to each other. Predictably, the SOA formation mechanism in the
386 presence of NO_X is different from that with $NO_X + NH_3$. In the absence of NH_3, the RO
387 intermediate, which is easily fragmented to produce relatively high-volatility
388 compounds, was the dominant product of the $NO_X + RO_2$ reaction (Zhao et al., 2018;Liu
389 et al., 2019a;Xu et al., 2020). Highly volatile compounds cannot readily partition into

390 the particle-phase, which subsequently results in a lower SOA yield in the presence of
391 NO_X (Yang et al., 2020). Thereby, both OS_C and the SOA mass concentration were
392 lower when 60 ppb NO_X was added into the chamber. However, when both NO_X and
393 NH_3 were present, the toluene derived SOA had the lowest OS_C value, but the highest
394 mass concentration. This result suggested that although NO_X promotes the formation
395 of higher volatility compounds, these higher volatility compounds (e.g. glyoxal) can
396 react with NH_3 and partition into the particle-phase, which could contribute to the
397 increase in SOA formation. Huffman et al. (2009) observed that aerosol volatility was
398 inversely correlated with the extent of oxidation of OA components. The low value of
399 OS_C in the presence of NO_X indicated that NO_X would promote the formation of the
400 relatively high-volatility compounds. However, the lower OS_C value in the presence of
401 NH_3 indicated that the high-volatility compounds would promote partitioning into the
402 particle-phase when reacting with NH_3.

403 Fragments derived from the AMS data have also been widely used to explore the
404 bulk compositions and properties of SOA (Ng et al., 2010;Ng et al., 2017). The m/z 43
405 (f43) frequency was dominated by ion $C_2H_3O^+$, which is the tracer for organic
406 compounds with alcohol and carbonyl functional groups (Alfarra et al., 2006).
407 Meanwhile, the m/z 44 (f44) signal was dominated by CO_2^+ ions, which is the tracer
408 for organic compounds with carboxyl functional groups and an indicator of highly
409 oxygenated organic aerosols (Ng et al., 2010). Here, we use the approach of Ng et al.
410 (2010) by plotting the fractions of the total organic signal at m/z 43 *vs.* m/z 44 (f43 *vs.*
411 f44). The change of f43 *vs.* f44, which has an inflection point during the photooxidation

process, is shown in Fig. 3 and Fig. S3. In our study, the change before the inflection point was defined as the formation stage, and the linear fit of f43 *vs.* f44 for the formation stage is shown by the dashed lines. The change in f43 *vs.* f44 after the inflection point was defined as the stable stage, and the linear fit of f43 *vs.* f44 in this stage is shown by the solid lines. The formation and stable stages of the f43 *vs.* f44 relationship during the experiment are discussed separately here.

In the stable stage, the increase in f44 and decrease in f43 with increasing OH exposure indicated that the carbonyl groups in toluene SOA were oxidized to carboxyl groups by the ageing process. For the experiments without NH_3 and NO_X, the slope ratio of f43 *vs.* f44 was -3.9. When there was 60 ppb initial NO_X, the f43 was almost stable while the f44 increased with the oxidation process. There was a lower slope ratio of f43 *vs.* f44, indicating that organic compounds with more alcohol and carbonyl functional groups had formed in the presence of NO_X. But for the experiments with 200 ppb initial NH_3, the slope ratios of f43 *vs.* f44 were only -1.1 and -1.3 in the presence and absence of NO_X, respectively. According to the above results, we can see that more carbonyl groups are consumed as carboxyl groups are formed in the presence of NH_3. The carbonyls can be oxidized to organic acids (Kawamura and Bikkina, 2016), but unreacted carbonyl can be nucleophilically attacked by NH_3/NH_4^+ to form nitrogen-heterocyclic compounds, e.g., imidazole (Grace et al., 2019;Lian et al., 2020). Meanwhile, the peak f44 value decreased from 0.13 to 0.10 when NH_3 was added into the chamber. This suggested that the heterogeneous reaction of NH_3/NH_4^+ could promote the consumption of particle-phase carbonyl groups (Xu et al., 2018), and must

434 inhibit the formation of carboxyl groups in the SOA ageing process. According to the
435 changing trend of SOA concentration over time, the photooxidation process was
436 divided into formation stage and stable stage. As shown in Fig. 1, the first half hour of
437 photooxidation when SOA concentration increased linearly with time was defined as
438 SOA formation stage. After 60 min of photooxidation, SOA concentration was not
439 changed with reaction time, and it was defined as stable stage. The differences in spectra
440 of toluene SOA in the formation stage and stable stage are shown in Fig. 4. A lower
441 signal intensity variation of CO_2^+ in the presence of NH_3 also illustrated that NH_3 would
442 inhibit heterogeneous reactions that form carboxyl groups.

443 In the formation stage, the slope ratios of f43 *vs.* f44 were almost the same for both
444 experiments without NO_X. It can thus be seen that the presence or absence of NH_3 does
445 not affect the change trend of f43 *vs.* f44 in the SOA formation stage. Therefore, the
446 gas-phase homogeneous reaction of NH_3 on SOA formation is not important. Clearly,
447 the particle-phase heterogeneous reaction was the main reaction pathway by which NH_3
448 participated in the photooxidation process and toluene SOA formation. However,
449 negative correlations were observed between f43 and f44 in the presence of NO_X. Based
450 on this, we concluded that NO_X not only affects the SOA formation through the particle-
451 phase heterogeneous reactions, but also through gas-phase homogeneous reactions.

452 ## 3.3 PMF results

453 A temporal evaluation of the toluene SOA chemical composition during
454 photooxidation is vital to the analysis of the NOA formation mechanism in the presence

455 of NH_3 and/or NO_X. Therefore, this study further compared the chemical properties of
456 the SOA generated under different experimental conditions by applying a PMF analysis
457 to the HR-ToF-AMS data (Chen et al., 2019). A summary of the PMF results is
458 presented in Fig. S4-S7. For the toluene OH-photooxidation experiments with NH_3
459 and/or NO_X presence, two factors were identified from the PMF analysis in the same
460 way of Chen et al. (2019). The H/C, O/C, and N/C values of these two factors are shown
461 in Fig. 5. The factor with higher N/C values was defined as high-nitrogen OA (Hi-NOA).
462 In contrast, the factor with lower N/C values was defined as low-nitrogen OA (Lo-
463 NOA). Fig. 6 exhibits the evolution of Hi-NOA and Lo-NOA during the photooxidation
464 process as resolved from the PMF analysis of different initial NO_X/NH_3 concentrations.
465 While similar evolutionary trends were observed under different conditions, the relative
466 intensities and the chemical compositions of these two factors in each experiment were
467 not consistent.

468 For the toluene SOA formed under NH_3 conditions, both Lo-NOA and Hi-NOA
469 had similar O/C values, which were fully oxygenated with an average of 0.74 ± 0.04
470 (Fig. 5a). These O/C values were comparable to the low-volatility oxygenated organic
471 aerosols (LV-OOA) with an O/C value ranging from 0.6 to 1 (Jimenez et al., 2009). The
472 main difference between these two OA sources was the N/C ratio. The N/C ratio of Hi-
473 NOA (N/C = 0.032) was about three times higher than that of Lo-NOA (N/C = 0.010)
474 (Fig. 5a). The evolution of these two OA sources during the photooxidation process is
475 shown in Fig. 6a. The components of toluene SOA were mostly Lo-NOA during the
476 initial phase of SOA formation, but Hi-NOA toluene SOA started forming after 10

minutes and continued to increase. The Lo-NOA reached the maximum mass concentration after 30 min of the photooxidation, and then decreased. Such a declining trend of Lo-NOA at longer reaction times reflected the conversion of Lo-NOA into something else in the particle-phase. As the Lo-NOA decreased, the mass concentration of Hi-NOA gradually increased. Thus, the Hi-NOA should be derived from the heterogeneous reaction of Lo-NOA with NH_3/NH_4^+. At the same time, it was proved that the formation pathway of Hi-NOA was not through reaction of NH_3 with later-generation gas-phase products in the homogeneous gas phase. With the gradual replacement of Lo-NOA by Hi-NOA, the ratio of [Hi-NOA]/[Lo-NOA] stabilized at 5~6.

For the toluene SOA formed under NO_X conditions, there was not a large difference between the N/C ratios of Hi-NOA (N/C = 0.019) and Lo-NOA (N/C = 0.014) (Fig. 5c). At the end of the NO_X experiment, the ratio of [Hi-NOA]/[Lo-NOA] was only 3:2 (Fig. 6c). It follows that the contribution of the heterogeneous NO_X reaction to the N/C ratio of toluene SOA was not obvious. Therefore, the formation of NOA in the presence of NO_X mainly occurred through gas-phase homogeneous reactions, which was consistent with the results in section 3.3.

The changing trend of N/C with time in the presence of NH_3 was different to that with NO_X present. The evolutions of the N/C of SOA in different experiments are shown in Fig. 7. In the presence of NH_3, the N/C value gradually increased throughout the photooxidation process. The increased N/C value in the photooxidation process was attributed to the heterogeneous NH_3 reaction with SOA. But in the presence of NO_X,

499 the N/C increased rapidly to its maximum value where it was stable for the rest of the
500 reaction. This could mean that the heterogeneous reaction of toluene SOA with NO_X to
501 form NOA was not as important as the gas-phase homogeneous reaction.

502 When both NO_X and NH_3 were added into the chamber, the N/C ratios of Hi-NOA
503 and Lo-NOA were 0.062 and 0.029, respectively (Fig. 5b). The N/C ratio of Hi-NOA,
504 which was comparable to the recently isolated nitrogen-enriched OA value (0.053)
505 observed by Sun et al. (2011), was much higher than that observed in the experiments
506 with only NH_3 or NO_X. It was even higher than the sum of the N/C ratios from both
507 Exp. 2 with NH_3 and Exp. 4 with NO_X. In order to calculate the relative contributions
508 of NH_3 and NO_X to N/C, it was assumed that the effects of NH_3 or NO_X on the N/C
509 ratio in the Hi-NOA and Lo-NOA factors did not change among different experimental
510 conditions. For Lo-NOA, the contributions of NH_3 and NO_X to the N/C value were
511 0.0126 and 0.0164, and their relative intensities were 43% and 57%, respectively. While
512 for the Hi-NOA, the contributions of NH_3 and NO_X to the N/C values were 0.0404 and
513 0.0216, and their relative intensities were 65% and 35%, respectively. For the
514 experiment with both NH_3 and NO_X, the contribution of NH_3 to N/C was higher by 26%,
515 and the contribution of NO_X to N/C was higher by 17% compared to the experiments
516 with the single pollutants. The co-existence of NH_3 and NO_X further enhanced the N/C
517 value of toluene SOA, indicating that a synergetic interaction between NH_3 and NO_X
518 further enhanced organic nitrogen formation.

3.4 Optical absorption

The optical characteristics of toluene SOA formed from different NH_3 and NO_X conditions were investigated. The MAC of toluene derived SOA detected over the range of 230–600 nm is displayed in Fig. 8. Over the entire UV detection range, an increase in light absorption was observed when the toluene SOA formed in the presence of NO_X or NH_3.

By looking at Fig. 8 in detail, one can see that the MAC of toluene SOA formed with (red line) and without (black line) NH_3 overlapped at 250 nm, but when the UV wavelength exceeded 250 nm the MAC of the toluene SOA formed in the presence of NH_3 was higher. The red line reflects an obvious characteristic absorption peak at 270~280 nm, which was mainly due to the absorption of the $n\rightarrow\pi^*$ electronic transitions. The imidazole compounds were formed through the Maillard reactions between NH_3/NH_4^+ with carbonyl functional groups (Zhang et al., 2015a). The C=N double bonds in the organonitrogen imidazole compounds can act as effective chromophores since both $\pi\rightarrow\pi^*$ and $n\rightarrow\pi^*$ transitions are chromatically active (Nguyen et al., 2013). The UV/visible spectrum of imine and pyrrole show broad bands at 270 nm (NIST, 2020), which was consistent with the UV absorption peak of the $n\rightarrow\pi^*$ band observed here. According to the AMS results, carbonyl was the main functional group of toluene SOA. The emergence of absorption peaks at 270~280 nm demonstrated that some organonitrogen imidazole compounds (e.g. imines and pyrrole) were formed through the heterogeneous reaction of toluene with NH_3. Meanwhile, the

high-molecular weight nitrogen-containing organic species might have formed through Maillard reactions in the particle-phase (Wang et al., 2010). This was also a reason for the increase in SOA mass concentration in the presence of NH_3.

The green line in Fig. 8 represents the MAC value of toluene-derived SOA in the presence of NO_X, which was also higher than the black line (control) throughout the UV detection range. When compared with the red line, the green line had no obvious characteristic peak at 280 nm, but it had higher absorbance in the range between 240 and 280 nm. This indicated that both NO_X and NH_3 increased the absorbance of toluene SOA, while the chromophores generated from the reactions between toluene-derived SOA with NH_3 or NO_X did not behave in the same way.

The blue line in Fig. 8 represents the absorbance of toluene SOA formed in the presence of both NO_X and NH_3. The MAC of toluene SOA formed in the presence of both NO_X and NH_3 was higher than the toluene SOA formed in the presence of either NH_3 or NO_X. There might have been a synergetic effect between NO_X and NH_3 on the absorbance of toluene SOA. Considering that the mass concentration of toluene SOA formed in the presence of both NH_3 and NO_X was the highest, as described in section 3.1, the co-existence of NH_3 and NO_X may also result in the toluene SOA having stronger light absorption and atmospheric radiative forcing. We also noted a higher MAC value at 280 nm, which illustrated that the presence of NO_X could promote the formation of imines and pyrrole in the photooxidation system of toluene with NH_3.

4 Conclusion

Here we present the results of a study in which we characterized the mass concentrations, chemical compositions, and optical properties of SOA formed from the photooxidation of toluene under different NH_3 and NO_X concentrations. When compared with the control experiment, the SOA mass concentration data showed that the formation of toluene-derived SOA was enhanced in the presence of NH_3, through acid-base reactions between carboxyl groups or Maillard reactions with carbonyls, but inhibited in the presence of NO_X. Meanwhile, the mass concentration of toluene SOA formed in the presence of both NO_X and NH_3 was higher than those formed under either NH_3 or NO_X alone. This result indicated that there was a synergistic interaction between NH_3 and NO_X that further enhanced toluene-derived SOA formation. At the same time, the lowest OS_C value was obtained when both NH_3 and NO_X were present. We concluded that highly volatile compounds, which were formed from toluene photooxidation in the presence of NO_X, could react with NH_3 to form products with lower volatilities, and promoted the partitioning of these products into the particle-phase.

Synergetic effects of NH_3 and NO_X on the formation of NOA and the optical properties of SOA were also observed in this study. The heterogeneous reaction was responsible for the formation of NOA in the presence of NH_3. Meanwhile, an absorption peak at 270~280 nm, which is characteristic of imine and pyrrole, was observed. In contrast, the formation of NOA caused by NO_X alone was mainly due to a gas phase homogeneous reaction.

In the actual atmosphere especially in Chinese urban atmosphere, NO_X and NH_3 abundantly co-exist. Therefore, the findings presented here clearly show that the synergetic effects of NO_X and NH_3 should not be neglected. In the meantime, our work provides a scientific basis for the consideration of synergistic emission reductions of NH_3 and NO_X under the compound pollution conditions, which will contribute to reducing the burden of aerosols in the atmosphere. It has to be noted that the concentration of reactants used for the experiments is much higher than that observed in polluted areas. Although the reactant concentrations including NH_3 used in this work are much higher than those in the real urban environment, our results are applicable for the polluted urban atmosphere. In the urban atmosphere aromatic VOCs consist of numerous species and their total concentration is much higher than a single species such as toluene. On the other hand, carboxylic acids and carbonyls in the urban polluted atmosphere can be produced from aromatics and many other species. Therefore, it is reasonable for our smog chamber experiments to use toluene as a single precursor with a concentration much higher than that in the real atmosphere. Although the mechanisms of SOA formed under high precursor concentrations is expected to be the same as that under low concentrations, the kinetics are probably different. Thus, the effect of NH_3 and NO_X on the photooxidation of toluene with lower concentrations should be checked in the further study.

Data availability

The datasets are available from https://doi.org/10.6084/m9.figshare.16910953.

Author contributions

SL and GW designed the experiment. SL, DH and YW conducted the experiments. SL, DH, YW and GW performed the data interpretation. SL and GW wrote the paper. YW, SZ, XL, CW, WD contributed to the paper with useful scientific discussions or comments.

Competing interests

The authors declare that they have no conflict of interest.

Acknowledgements

This work was financially supported by National Natural Science Foundation of China (Grant No. 42130704, 42005088); the China Postdoctoral Science Foundation (Grant No. 2019M661427); Fundamental Research Funds for the Central Universities, Director's Fund of Key Laboratory of Geographic Information Science (Ministry of Education), East China Normal University (Grant No. KLGIS2021C02); and ECNU Happiness Flower Program.

Reference

Alfarra, M. R., Paulsen, D., Gysel, M., Garforth, A. A., Dommen, J., Prevot, A. S. H., Worsnop, D. R., Baltensperger, U., and Coe, H.: A mass spectrometric study of secondary organic aerosols formed from the photooxidation of anthropogenic and biogenic precursors in a reaction chamber, Atmos. Chem. Phys., 6, 5279-5293, DOI 10.5194/acp-6-5279-2006, 2006.

Babar, Z. B., Park, J.-H., and Lim, H.-J.: Influence of NH_3 on secondary organic aerosols from the ozonolysis and photooxidation of α-pinene in a flow reactor, Atmos. Environ., 164, 71-84, 10.1016/j.atmosenv.2017.05.034, 2017.

Bates, K., Jacob, D., Li, K., Ivatt, P., Evans, M., Yan, Y., and Lin, J.: Development and evaluation of a new compact mechanism for aromatic oxidation in atmospheric models, Atmos. Chem. Phys. Discuss., 2021, 1-34, 10.5194/acp-2021-605, 2021.

Berkemeier, T., Ammann, M., Mentel, T. F., Poschl, U., and Shiraiwa, M.: Organic nitrate contribution to new particle formation and growth in secondary organic aerosols from α-pinene ozonolysis, Environ. Sci. Technol., 50, 6334-6342, 10.1021/acs.est.6b00961, 2016.

633 Chen, C. L., Li, L. J., Tang, P., and Cocker, D. R.: SOA formation from photooxidation of naphthalene
634 and methylnaphthalenes with m-xylene and surrogate mixtures, Atmos. Environ., 180, 256-264,
635 10.1016/j.atmosenv.2018.02.051, 2018.

636 Chen, T. Z., Liu, Y. C., Ma, Q. X., Chu, B. W., Zhang, P., Liu, C. G., Liu, J., and He, H.: Significant
637 source of secondary aerosol: formation from gasoline evaporative emissions in the presence of SO_2
638 and NH_3, Atmos. Chem. Phys., 19, 8063-8081, 10.5194/acp-19-8063-2019, 2019.

639 Chen, Y., and Bond, T. C.: Light absorption by organic carbon from wood combustion, Atmos. Chem.
640 Phys., 10, 1773-1787, 10.5194/acp-10-1773-2010, 2010.

641 Chu, B. W., Zhang, X., Liu, Y. C., He, H., Sun, Y., Jiang, J. K., Li, J. H., and Hao, J. M.: Synergetic
642 formation of secondary inorganic and organic aerosol: effect of SO_2 and NH_3 on particle formation
643 and growth, Atmos. Chem. Phys., 16, 14219-14230, 10.5194/acp-16-14219-2016, 2016.

644 de Foy, B., Lu, Z., and Streets, D. G.: Satellite NO_2 retrievals suggest China has exceeded its NO_X
645 reduction goals from the twelfth Five-Year Plan, Sci. Rep., 6, 35912, 10.1038/srep35912, 2016.

646 Draper, D. C., Farmer, D. K., Desyaterik, Y., and Fry, J. L.: A qualitative comparison of secondary organic
647 aerosol yields and composition from ozonolysis of monoterpenes at varying concentrations of NO_2,
648 Atmos. Chem. Phys., 15, 12267-12281, 10.5194/acp-15-12267-2015, 2015.

649 Erisman, J. W., and Schaap, M.: The need for ammonia abatement with respect to secondary PM
650 reductions in Europe, Environ. Pollut., 129, 159-163, 10.1016/j.envpol.2003.08.042, 2004.

651 Ge, S., Wang, G., Zhang, S., Li, D., Xie, Y., Wu, C., Yuan, Q., Chen, J., and Zhang, H.: Abundant NH_3
652 in China enhances atmospheric HONO production by promoting the heterogeneous reaction of SO_2
653 with NO_2, Environ. Sci. Technol., 53, 14339-14347, 10.1021/acs.est.9b04196, 2019.

654 Grace, D. N., Sharp, J. R., Holappa, R. E., Lugos, E. N., Sebold, M. B., Griffith, D. R., Hendrickson, H.
655 P., and Galloway, M. M.: Heterocyclic product formation in aqueous brown carbon systems, ACS
656 Earth Space Chem., 3, 2472-2481, 10.1021/acsearthspacechem.9b00235, 2019.

657 Herndon, S. C., Onasch, T. B., Wood, E. C., Kroll, J. H., Canagaratna, M. R., Jayne, J. T., Zavala, M. A.,
658 Knighton, W. B., Mazzoleni, C., Dubey, M. K., Ulbrich, I. M., Jimenez, J. L., Seila, R., de Gouw, J.
659 A., de Foy, B., Fast, J., Molina, L. T., Kolb, C. E., and Worsnop, D. R.: Correlation of secondary
660 organic aerosol with odd oxygen in Mexico City, Geophys. Res. Lett., 35, Artn L15804,
661 10.1029/2008gl034058, 2008.

662 Huang, D. D., Zhang, X., Dalleska, N. F., Lignell, H., Coggon, M. M., Chan, C. M., Flagan, R. C.,
663 Seinfeld, J. H., and Chan, C. K.: A note on the effects of inorganic seed aerosol on the oxidation
664 state of secondary organic aerosol-α-Pinene ozonolysis, J Geophys Res-Atmos, 121, 12476-12483,
665 10.1002/2016jd025999, 2016.

666 Huang, Y., Lee, S. C., Ho, K. F., Ho, S. S. H., Cao, N. Y., Cheng, Y., and Gao, Y.: Effect of ammonia on
667 ozone-initiated formation of indoor secondary products with emissions from cleaning products,
668 Atmos. Environ., 59, 224-231, 10.1016/j.atmosenv.2012.04.059, 2012.

669 Huffman, J. A., Docherty, K. S., Mohr, C., Cubison, M. J., Ulbrich, I. M., Ziemann, P. J., Onasch, T. B.,
670 and Jimenez, J. L.: Chemically-resolved volatility measurements of organic aerosol fom different
671 sources, Environ. Sci. Technol., 43, 5351-5357, 10.1021/es803539d, 2009.

672 Jang, M., Czoschke, N. M., Lee, S., and Kamens, R. M.: Heterogeneous atmospheric aerosol production
673 by acid-catalyzed particle-phase reactions, Science, 298, 814-817, 10.1126/science.1075798, 2002.

674 Ji, Y., Zhao, J., Terazono, H., Misawa, K., Levitt, N. P., Li, Y., Lin, Y., Peng, J., Wang, Y., Duan, L., Pan,
675 B., Zhang, F., Feng, X., An, T., Marrero-Ortiz, W., Secrest, J., Zhang, A. L., Shibuya, K., Molina,
676 M. J., and Zhang, R.: Reassessing the atmospheric oxidation mechanism of toluene, Proc. Natl.
677 Acad. Sci. U. S. A., 114, 8169-8174, 10.1073/pnas.1705463114, 2017.

678 Jiang, X. T., Lv, C., You, B., Liu, Z. Y., Wang, X. F., and Du, L.: Joint impact of atmospheric SO_2 and
679 NH_3 on the formation of nanoparticles from photo-oxidation of a typical biomass burning compound,
680 Environ Sci-Nano, 7, 2532-2545, 10.1039/d0en00520g, 2020.

681 Jimenez, J. L., Canagaratna, M. R., Donahue, N. M., Prevot, A. S., Zhang, Q., Kroll, J. H., DeCarlo, P.

F., Allan, J. D., Coe, H., Ng, N. L., Aiken, A. C., Docherty, K. S., Ulbrich, I. M., Grieshop, A. P., Robinson, A. L., Duplissy, J., Smith, J. D., Wilson, K. R., Lanz, V. A., Hueglin, C., Sun, Y. L., Tian, J., Laaksonen, A., Raatikainen, T., Rautiainen, J., Vaattovaara, P., Ehn, M., Kulmala, M., Tomlinson, J. M., Collins, D. R., Cubison, M. J., Dunlea, E. J., Huffman, J. A., Onasch, T. B., Alfarra, M. R., Williams, P. I., Bower, K., Kondo, Y., Schneider, J., Drewnick, F., Borrmann, S., Weimer, S., Demerjian, K., Salcedo, D., Cottrell, L., Griffin, R., Takami, A., Miyoshi, T., Hatakeyama, S., Shimono, A., Sun, J. Y., Zhang, Y. M., Dzepina, K., Kimmel, J. R., Sueper, D., Jayne, J. T., Herndon, S. C., Trimborn, A. M., Williams, L. R., Wood, E. C., Middlebrook, A. M., Kolb, C. E., Baltensperger, U., and Worsnop, D. R.: Evolution of organic aerosols in the atmosphere, Science, 326, 1525-1529, 10.1126/science.1180353, 2009.

Kawamura, K., and Bikkina, S.: A review of dicarboxylic acids and related compounds in atmospheric aerosols: Molecular distributions, sources and transformation, Atmos. Res., 170, 140-160, 10.1016/j.atmosres.2015.11.018, 2016.

Kourtchev, I., Doussin, J. F., Giorio, C., Mahon, B., Wilson, E. M., Maurin, N., Pangui, E., Venables, D. S., Wenger, J. C., and Kalberer, M.: Molecular composition of fresh and aged secondary organic aerosol from a mixture of biogenic volatile compounds: a high-resolution mass spectrometry study, Atmos. Chem. Phys., 15, 5683-5695, 10.5194/acp-15-5683-2015, 2015.

Krechmer, J. E., Day, D. A., and Jimenez, J. L.: Always lost but never forgotten: Gas-phase wall losses are important in all teflon environmental chambers, Environ. Sci. Technol., 54, 12890-12897, 10.1021/acs.est.0c03381, 2020.

Kroll, J. H., Donahue, N. M., Jimenez, J. L., Kessler, S. H., Canagaratna, M. R., Wilson, K. R., Altieri, K. E., Mazzoleni, L. R., Wozniak, A. S., Bluhm, H., Mysak, E. R., Smith, J. D., Kolb, C. E., and Worsnop, D. R.: Carbon oxidation state as a metric for describing the chemistry of atmospheric organic aerosol, Nat. Chem., 3, 133-139, 10.1038/nchem.948, 2011.

Kuwata, M., and Martin, S. T.: Phase of atmospheric secondary organic material affects its reactivity, Proc. Natl. Acad. Sci. U. S. A., 109, 17354-17359, 10.1073/pnas.1209071109, 2012.

Laskin, A., Laskin, J., and Nizkorodov, S. A.: Chemistry of atmospheric brown carbon, Chem. Rev., 115, 4335-4382, 10.1021/cr5006167, 2015.

Laskin, J., Laskin, A., Roach, P. J., Slysz, G. W., Anderson, G. A., Nizkorodov, S. A., Bones, D. L., and Nguyen, L. Q.: High-resolution desorption electrospray ionization mass spectrometry for chemical characterization of organic aerosols, Anal. Chem., 82, 2048-2058, 10.1021/ac902801f, 2010.

Laskin, J., Laskin, A., Nizkorodov, S. A., Roach, P., Eckert, P., Gilles, M. K., Wang, B., Lee, H. J., and Hu, Q.: Molecular selectivity of brown carbon chromophores, Environ. Sci. Technol., 48, 12047-12055, 10.1021/es503432r, 2014.

Lee, A. K., Zhao, R., Li, R., Liggio, J., Li, S. M., and Abbatt, J. P.: Formation of light absorbing organo-nitrogen species from evaporation of droplets containing glyoxal and ammonium sulfate, Environ. Sci. Technol., 47, 12819-12826, 10.1021/es402687w, 2013.

Li, K., Chen, L., White, S. J., Yu, H., Wu, X., Gao, X., Azzi, M., and Cen, K.: Smog chamber study of the role of NH_3 in new particle formation from photo-oxidation of aromatic hydrocarbons, Sci. Total Environ., 619-620, 927-937, 10.1016/j.scitotenv.2017.11.180, 2018.

Lian, X., Zhang, G., Yang, Y., Lin, Q., Fu, Y., Jiang, F., Peng, L., Hu, X., Chen, D., Wang, X., Peng, P. a., Sheng, G., and Bi, X.: Evidence for the formation of imidazole from carbonyls and reduced nitrogen species at the individual particle level in the ambient atmosphere, Environ. Sci. Tech. Let., 10.1021/acs.estlett.0c00722, 2020.

Liu, M., Huang, X., Song, Y., Xu, T., Wang, S., Wu, Z., Hu, M., Zhang, L., Zhang, Q., Pan, Y., Liu, X., and Zhu, T.: Rapid SO_2 emission reductions significantly increase tropospheric ammonia concentrations over the North China Plain, Atmos. Chem. Phys., 18, 17933-17943, 10.5194/acp-18-17933-2018, 2018.

Liu, S. J., Jia, L., Xu, Y., Tsona, N. T., Ge, S. S., and Du, L.: Photooxidation of cyclohexene in the presence of SO_2: SOA yield and chemical composition, Atmos. Chem. Phys., 17, 13329-13343, 10.5194/acp-17-13329-2017, 2017.

Liu, S. J., Jiang, X. T., Tsona, N. T., Lv, C., and Du, L.: Effects of NO_X, SO_2 and RH on the SOA formation from cyclohexene photooxidation, Chemosphere, 216, 794-804, 10.1016/j.chemosphere.2018.10.180, 2019a.

Liu, S. J., Tsona, N. T., Zhang, Q., Jia, L., Xu, Y. F., and Du, L.: Influence of relative humidity on cyclohexene SOA formation from OH photooxidation, Chemosphere, 231, 478-486, 10.1016/j.chemosphere.2019.05.131, 2019b.

Liu, S. J., Wang, Y., Wang, G., Zhang, S., Li, D., Du, L., Wu, C., Du, W., and Ge, S.: Enhancing effect of NO_2 on the formation of light-absorbing secondary organic aerosols from toluene photooxidation, Sci. Total Environ., 794, 148714, 10.1016/j.scitotenv.2021.148714, 2021.

Liu, Y. C., Liggio, J., Staebler, R., and Li, S. M.: Reactive uptake of ammonia to secondary organic aerosols: Kinetics of organonitrogen formation, Atmos. Chem. Phys., 15, 13569-13584, 10.5194/acp-15-13569-2015, 2015.

Ma, P., Zhang, P., Shu, J., Yang, B., and Zhang, H.: Characterization of secondary organic aerosol from photo-oxidation of gasoline exhaust and specific sources of major components, Environ. Pollut., 232, 65-72, 10.1016/j.envpol.2017.09.018, 2018a.

Ma, Q., Lin, X., Yang, C., Long, B., Gai, Y., and Zhang, W.: The influences of ammonia on aerosol formation in the ozonolysis of styrene: Roles of Criegee intermediate reactions, R. Soc. Open Sci., 5, 172171, 10.1098/rsos.172171, 2018b.

Malecha, K. T., and Nizkorodov, S. A.: Photodegradation of secondary organic aerosol particles as a source of small, oxygenated volatile organic compounds, Environ. Sci. Technol., 50, 9990-9997, 10.1021/acs.est.6b02313, 2016.

Mandariya, A. K., Gupta, T., and Tripathi, S. N.: Effect of aqueous-phase processing on the formation and evolution of organic aerosol (OA) under different stages of fog life cycles, Atmos. Environ., 206, 60-71, 10.1016/j.atmosenv.2019.02.047, 2019.

Middlebrook, A. M., Bahreini, R., Jimenez, J. L., and Canagaratna, M. R.: Evaluation of composition-dependent collection efficiencies for the aerodyne aerosol mass spectrometer using field data, Aerosol Sci. Tech., 46, 258-271, 10.1080/02786826.2011.620041, 2012.

Moise, T., Flores, J. M., and Rudich, Y.: Optical properties of secondary organic aerosols and their changes by chemical processes, Chem. Rev., 115, 4400-4439, 10.1021/cr5005259, 2015.

Na, K., Song, C., Switzer, C., and Cocker, D. R.: Effect of ammonia on secondary organic aerosol formation from α-pinene ozonolysis in dry and humid conditions, Environ. Sci. Technol., 41, 6096-6102, 10.1021/es061956y, 2007.

Ng, N. L., Chhabra, P. S., Chan, A. W. H., Surratt, J. D., Kroll, J. H., Kwan, A. J., McCabe, D. C., Wennberg, P. O., Sorooshian, A., Murphy, S. M., Dalleska, N. F., Flagan, R. C., and Seinfeld, J. H.: Effect of NO_X level on secondary organic aerosol (SOA) formation from the photooxidation of terpenes, Atmos. Chem. Phys., 7, 5159-5174, 10.5194/acp-7-5159-2007, 2007a.

Ng, N. L., Kroll, J. H., Chan, A. W. H., Chhabra, P. S., Flagan, R. C., and Seinfeld, J. H.: Secondary organic aerosol formation from m-xylene, toluene, and benzene, Atmos. Chem. Phys., 7, 3909-3922, 10.5194/acp-7-3909-2007, 2007b.

Ng, N. L., Canagaratna, M. R., Zhang, Q., Jimenez, J. L., Tian, J., Ulbrich, I. M., Kroll, J. H., Docherty, K. S., Chhabra, P. S., Bahreini, R., Murphy, S. M., Seinfeld, J. H., Hildebrandt, L., Donahue, N. M., DeCarlo, P. F., Lanz, V. A., Prévôt, A. S. H., Dinar, E., Rudich, Y., and Worsnop, D. R.: Organic aerosol components observed in Northern Hemispheric datasets from Aerosol Mass Spectrometry, Atmos. Chem. Phys., 10, 4625-4641, 10.5194/acp-10-4625-2010, 2010.

Ng, N. L., Brown, S. S., Archibald, A. T., Atlas, E., Cohen, R. C., Crowley, J. N., Day, D. A., Donahue, N. M., Fry, J. L., Fuchs, H., Griffin, R. J., Guzman, M. I., Herrmann, H., Hodzic, A., Iinuma, Y., Jimenez, J. L., Kiendler-Scharr, A., Lee, B. H., Luecken, D. J., Mao, J., McLaren, R., Mutzel, A., Osthoff, H. D., Ouyang, B., Picquet-Varrault, B., Platt, U., Pye, H. O. T., Rudich, Y., Schwantes, R. H., Shiraiwa, M., Stutz, J., Thornton, J. A., Tilgner, A., Williams, B. J., and Zaveri, R. A.: Nitrate radicals and biogenic volatile organic compounds: Oxidation, mechanisms, and organic aerosol, Atmos. Chem. Phys., 17, 2103-2162, 10.5194/acp-17-2103-2017, 2017.

784 Nguyen, T. B., Laskin, A., Laskin, J., and Nizkorodov, S. A.: Brown carbon formation from
785 ketoaldehydes of biogenic monoterpenest, Faraday Discuss., 165, 473-494, 10.1039/c3fd00036b,
786 2013.

787 NIST: NIST Chemistry WebBook Standard Reference Database 69, https://doi.org/10.18434/T4D303,
788 2020.

789 Noziere, B., Dziedzic, P., and Cordova, A.: Products and kinetics of the liquid-phase reaction of glyoxal
790 catalyzed by ammonium ions (NH_4^+), J. Phys. Chem. A, 113, 231-237, 10.1021/jp8078293, 2009.

791 Ortiz-Montalvo, D. L., Hakkinen, S. A., Schwier, A. N., Lim, Y. B., McNeill, V. F., and Turpin, B. J.:
792 Ammonium addition (and aerosol pH) has a dramatic impact on the volatility and yield of glyoxal
793 secondary organic aerosol, Environ. Sci. Technol., 48, 255-262, 10.1021/es4035667, 2014.

794 Paciga, A. L., Riipinen, I., and Pandis, S. N.: Effect of ammonia on the volatility of organic diacids,
795 Environ. Sci. Technol., 48, 13769-13775, 10.1021/es5037805, 2014.

796 Pathak, R. K., Stanier, C. O., Donahue, N. M., and Pandis, S. N.: Ozonolysis of alpha-pinene at
797 atmospherically relevant concentrations: Temperature dependence of aerosol mass fractions (yields),
798 J Geophys Res-Atmos, 112, Artn D03201, 10.1029/2006jd007436, 2007.

799 Peng, C., Yang, F., Tian, M., Shi, G., Li, L., Huang, R. J., Yao, X., Luo, B., Zhai, C., and Chen, Y.: Brown
800 carbon aerosol in two megacities in the Sichuan Basin of southwestern China: Light absorption
801 properties and implications, Sci. Total Environ., 719, 137483, 10.1016/j.scitotenv.2020.137483,
802 2020.

803 Prinn, R. G., Weiss, R. F., Miller, B. R., Huang, J., Alyea, F. N., Cunnold, D. M., Fraser, P. J., Hartley, D.
804 E., and Simmonds, P. G.: Atmospheric trends and lifetime of CH_3CCI_3 and global OH
805 concentrations, Science, 269, 187-192, 10.1126/science.269.5221.187, 1995.

806 Qi, X., Zhu, S., Zhu, C., Hu, J., Lou, S., Xu, L., Dong, J., and Cheng, P.: Smog chamber study of the
807 effects of NO_X and NH_3 on the formation of secondary organic aerosols and optical properties from
808 photo-oxidation of toluene, Sci. Total Environ., 727, 138632, 10.1016/j.scitotenv.2020.138632,
809 2020.

810 Sarrafzadeh, M., Wildt, J., Pullinen, I., Springer, M., Kleist, E., Tillmann, R., Schmitt, S. H., Wu, C.,
811 Mentel, T. F., Zhao, D. F., Hastie, D. R., and Kiendler-Scharr, A.: Impact of NO_X and OH on
812 secondary organic aerosol formation from β-pinene photooxidation, Atmos. Chem. Phys., 16,
813 11237-11248, 10.5194/acp-16-11237-2016, 2016.

814 Sun, Y. L., Zhang, Q., Schwab, J. J., Demerjian, K. L., Chen, W. N., Bae, M. S., Hung, H. M., Hogrefe,
815 O., Frank, B., Rattigan, O. V., and Lin, Y. C.: Characterization of the sources and processes of
816 organic and inorganic aerosols in New York city with a high-resolution time-of-flight aerosol mass
817 apectrometer, Atmos. Chem. Phys., 11, 1581-1602, 10.5194/acp-11-1581-2011, 2011.

818 Surratt, J. D., Murphy, S. M., Kroll, J. H., Ng, N. L., Hildebrandt, L., Sorooshian, A., Szmigielski, R.,
819 Vermeylen, R., Maenhaut, W., Claeys, M., Flagan, R. C., and Seinfeld, J. H.: Chemical composition
820 of secondary organic aerosol formed from the photooxidation of isoprene, J. Phys. Chem. A, 110,
821 9665-9690, 10.1021/jp061734m, 2006.

822 Volkamer, R., Jimenez, J. L., San Martini, F., Dzepina, K., Zhang, Q., Salcedo, D., Molina, L. T., Worsnop,
823 D. R., and Molina, M. J.: Secondary organic aerosol formation from anthropogenic air pollution:
824 Rapid and higher than expected, Geophys. Res. Lett., 33, Artn L17811, 10.1029/2006gl026899,
825 2006.

826 Vu, T. V., Shi, Z., Cheng, J., Zhang, Q., He, K., Wang, S., and Harrison, R. M.: Assessing the impact of
827 clean air action on air quality trends in Beijing using a machine learning technique, Atmos. Chem.
828 Phys., 19, 11303-11314, 10.5194/acp-19-11303-2019, 2019.

829 Wang, G., Zhang, F., Peng, J., Duan, L., Ji, Y., Marrero-Ortiz, W., Wang, J., Li, J., Wu, C., Cao, C., Wang,
830 Y., Zheng, J., Secrest, J., Li, Y., Wang, Y., Li, H., Li, N., and Zhang, R.: Particle acidity and sulfate
831 production during severe haze events in China cannot be reliably inferred by assuming a mixture of
832 inorganic salts, Atmos. Chem. Phys., 18, 10123-10132, 10.5194/acp-18-10123-2018, 2018a.

833 Wang, G. H., Zhang, R. Y., Gomez, M. E., Yang, L. X., Zamora, M. L., Hu, M., Lin, Y., Peng, J. F., Guo,

S., Meng, J. J., Li, J. J., Cheng, C. L., Hu, T. F., Ren, Y. Q., Wang, Y. S., Gao, J., Cao, J. J., An, Z. S., Zhou, W. J., Li, G. H., Wang, J. Y., Tian, P. F., Marrero-Ortiz, W., Secrest, J., Du, Z. F., Zheng, J., Shang, D. J., Zeng, L. M., Shao, M., Wang, W. G., Huang, Y., Wang, Y., Zhu, Y. J., Li, Y. X., Hu, J. X., Pan, B., Cai, L., Cheng, Y. T., Ji, Y. M., Zhang, F., Rosenfeld, D., Liss, P. S., Duce, R. A., Kolb, C. E., and Molina, M. J.: Persistent sulfate formation from London Fog to Chinese haze, Proc. Natl. Acad. Sci. U. S. A., 113, 13630-13635, 10.1073/pnas.1616540113, 2016.

Wang, R. Y., Ye, X. N., Liu, Y. X., Li, H. W., Yang, X., Chen, J. M., Gao, W., and Yin, Z.: Characteristics of atmospheric ammonia and its relationship with vehicle emissions in a megacity in China, Atmos. Environ., 182, 97-104, 10.1016/j.atmosenv.2018.03.047, 2018b.

Wang, S. W., Zhang, Q., Martin, R. V., Philip, S., Liu, F., Li, M., Jiang, X. T., and He, K. B.: Satellite measurements oversee China's sulfur dioxide emission reductions from coal-fired power plants, Environ. Res. Lett., 10, 114015, 10.1088/1748-9326/10/11/114015, 2015.

Wang, X., Gao, S., Yang, X., Chen, H., Chen, J., Zhuang, G., Surratt, J. D., Chan, M. N., and Seinfeld, J. H.: Evidence for high molecular weight nitrogen-containing organic salts in urban aerosols, Environ. Sci. Technol., 44, 4441-4446, 10.1021/es1001117, 2010.

Wang, Y., Chen, Y., Wu, Z., Shang, D., Bian, Y., Du, Z., Schmitt, S. H., Su, R., Gkatzelis, G. I., Schlag, P., Hohaus, T., Voliotis, A., Lu, K., Zeng, L., Zhao, C., Alfarra, M. R., McFiggans, G., Wiedensohler, A., Kiendler-Scharr, A., Zhang, Y., and Hu, M.: Mutual promotion between aerosol particle liquid water and particulate nitrate enhancement leads to severe nitrate-dominated particulate matter pollution and low visibility, Atmos. Chem. Phys., 20, 2161-2175, 10.5194/acp-20-2161-2020, 2020.

Wu, C., Zhang, S., Wang, G., Lv, S., Li, D., Liu, L., Li, J., Liu, S., Du, W., Meng, J., Qiao, L., Zhou, M., Huang, C., and Wang, H.: Efficient heterogeneous formation of ammonium nitrate on the saline mineral particle surface in the atmosphere of east asia during dust storm periods, Environ. Sci. Technol., 54, 15622-15630, 10.1021/acs.est.0c04544, 2020.

Xia, Y., Zhao, Y., and Nielsen, C. P.: Benefits of China's efforts in gaseous pollutant control indicated by the bottom-up emissions and satellite observations 2000-2014, Atmos. Environ., 136, 43-53, 10.1016/j.atmosenv.2016.04.013, 2016.

Xie, M., Chen, X., Hays, M. D., Lewandowski, M., Offenberg, J., Kleindienst, T. E., and Holder, A. L.: Light absorption of secondary organic aerosol: Composition and contribution of nitroaromatic compounds, Environ. Sci. Technol., 51, 11607-11616, 10.1021/acs.est.7b03263, 2017.

Xu, J., Huang, M. Q., Cai, S. Y., Liao, Y. M., Hu, C. J., Zhao, W. X., Gu, X. J., and Zhang, W. J.: Chemical composition and reaction mechanisms for aged p-xylene secondary organic aerosol in the presence of ammonia, J. Chin. Chem. Soc., 65, 578-590, 10.1002/jccs.201700249, 2018.

Xu, L., Kollman, M. S., Song, C., Shilling, J. E., and Ng, N. L.: Effects of NO_X on the volatility of secondary organic aerosol from isoprene photooxidation, Environ. Sci. Technol., 48, 2253-2262, 10.1021/es404842g, 2014.

Xu, L., Moller, K. H., Crounse, J. D., Kjaergaard, H. G., and Wennberg, P. O.: New insights into the radical chemistry and product distribution in the OH-initiated oxidation of benzene, Environ. Sci. Technol., 54, 13467-13477, 10.1021/acs.est.0c04780, 2020.

Yang, W. Y., Li, J., Wang, M., Sun, Y. L., and Wang, Z. F.: A case study of investigating secondary organic aerosol formation pathways in beijing using an observation-based SOA box model, Aerosol Air Qual. Res., 18, 1606-1616, 10.4209/aaqr.2017.10.0415, 2018.

Yang, Y., Vance, M., Tou, F. Y., Tiwari, A., Liu, M., and Hochella, M. F.: Nanoparticles in road dust from impervious urban surfaces: Distribution, identification, and environmental implications, Environ Sci-Nano, 3, 534-544, 10.1039/c6en00056h, 2016.

Yang, Z., Tsona, N. T., Li, J., Wang, S., Xu, L., You, B., and Du, L.: Effects of NO_X and SO_2 on the secondary organic aerosol formation from the photooxidation of 1,3,5-trimethylbenzene: A new source of organosulfates, Environ. Pollut., 264, 114742, 10.1016/j.envpol.2020.114742, 2020.

Zhang, L., Wang, Y., Feng, C., Liang, S., Liu, Y., Du, H., and Jia, N.: Understanding the industrial NO_X and SO_2 pollutant emissions in China from sector linkage perspective, Sci. Total Environ., 770, 145242, 10.1016/j.scitotenv.2021.145242, 2021a.

Zhang, Q., Jimenez, J. L., Canagaratna, M. R., Ulbrich, I. M., Ng, N. L., Worsnop, D. R., and Sun, Y.: Understanding atmospheric organic aerosols via factor analysis of aerosol mass spectrometry: a review, Anal. Bioanal. Chem., 401, 3045-3067, 10.1007/s00216-011-5355-y, 2011.

Zhang, R., Wang, G., Guo, S., Zamora, M. L., Ying, Q., Lin, Y., Wang, W., Hu, M., and Wang, Y.: Formation of urban fine particulate matter, Chem. Rev., 115, 3803-3855, 10.1021/acs.chemrev.5b00067, 2015a.

Zhang, S., Li, D., Ge, S., Liu, S., Wu, C., Wang, Y., Chen, Y., Lv, S., Wang, F., Meng, J., and Wang, G.: Rapid sulfate formation from synergetic oxidation of SO_2 by O_3 and NO_2 under ammonia-rich conditions: Implications for the explosive growth of atmospheric $PM_{2.5}$ during haze events in China, Sci. Total Environ., 772, 144897, 10.1016/j.scitotenv.2020.144897, 2021b.

Zhang, X., Cappa, C. D., Jathar, S. H., McVay, R. C., Ensberg, J. J., Kleeman, M. J., and Seinfeld, J. H.: Influence of vapor wall loss in laboratory chambers on yields of secondary organic aerosol, Proc. Natl. Acad. Sci. U. S. A., 111, 5802-5807, 10.1073/pnas.1404727111, 2014.

Zhang, X., Schwantes, R. H., McVay, R. C., Lignell, H., Coggon, M. M., Flagan, R. C., and Seinfeld, J. H.: Vapor wall deposition in Teflon chambers, Atmos. Chem. Phys., 15, 4197-4214, 10.5194/acp-15-4197-2015, 2015b.

Zhao, D. F., Schmitt, S. H., Wang, M. J., Acir, I. H., Tillmann, R., Tan, Z. F., Novelli, A., Fuchs, H., Pullinen, I., Wegener, R., Rohrer, F., Wildt, J., Kiendler-Scharr, A., Wahner, A., and Mentel, T. F.: Effects of NO_X and SO_2 on the secondary organic aerosol formation from photooxidation of α-pinene and limonene, Atmos. Chem. Phys., 18, 1611-1628, 10.5194/acp-18-1611-2018, 2018.

Zou, Y., Deng, X. J., Zhu, D., Gong, D. C., Wang, H., Li, F., Tan, H. B., Deng, T., Mai, B. R., Liu, X. T., and Wang, B. G.: Characteristics of 1 year of observational data of VOCs, NO_X and O_3 at a suburban site in Guangzhou, China, Atmos. Chem. Phys., 15, 6625-6636, 10.5194/acp-15-6625-2015, 2015.

Tables

Table 1. Summary of experimental conditions in this study

No.	Tol_0 (ppb)	Δ Tol (ppb)	NH_3[a] (ppb)	NO_2 (ppb)	RH (%)	SOA mass conc.[b,c] (μg m^{-3})	SOA yield[b] (%)
Exp.1	664.1	551.2	-	-	25 ± 1	637 ± 14.6	28.1
Exp.2	618.7	499.4	~200	-	23 ± 1	867 ± 12.7	34.7
Exp.3	620.9	526.1	~200	62	26 ± 1	1020 ± 10.6	42.7
Exp.4	645.7	539.5	-	63	25 ± 1	452 ± 18.9	19.5

[a] The concentration of NH_3 is estimated by the amount of NH_3 added and the volume of the smog chamber. [b] SOA concentration and yield were calculated after taking into account the wall loss. [c] The reported SOA mass concentrations was the peak values after the wall loss correction.

Figures

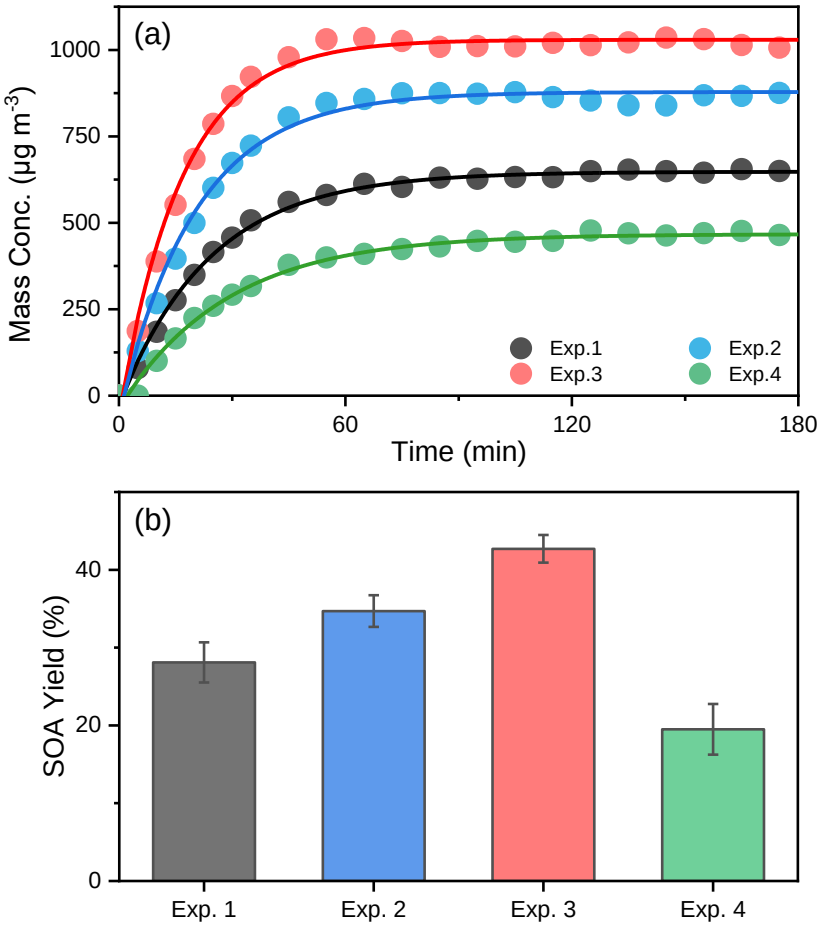

Fig. 1. The evolution of mass concentration (a) and yield (b) of toluene-derived SOA in different experiments. All the mass concentrations were wall-loss corrected. The error bars were calculated by the fluctuation of measured SOA concentration after the UV light was turn off at the end of each experiment

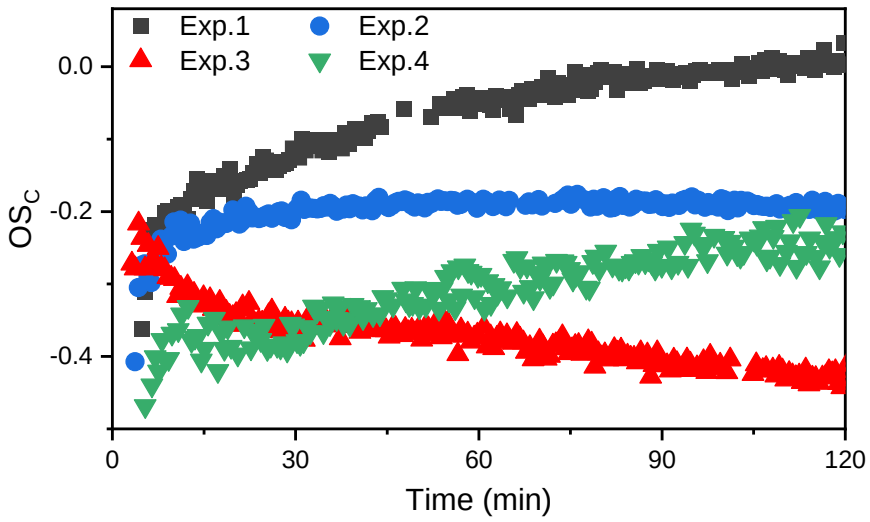

924

925 **Fig. 2.** The OS_C values for the toluene SOA formed under different NH_3/NO_X conditions.

926

927

928

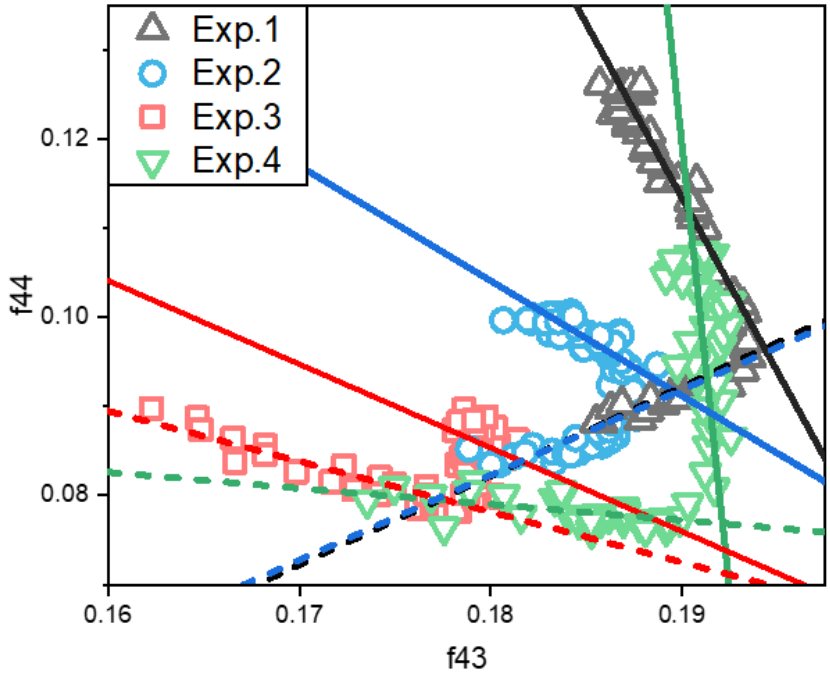

929

930 **Fig. 3.** The relationship between total organic signals at 43 m/z (f43) *vs.* 44 m/z (f44) from SOA
931 data during the photooxidation process. The f43 *vs.* f44 plots exhibited inflection points during the
932 photooxidation process. The dashed lines indicate the trends of f43 *vs.* f44 for the SOA formation
933 stage (before the inflection point) and the solid lines for the stable stage.

934

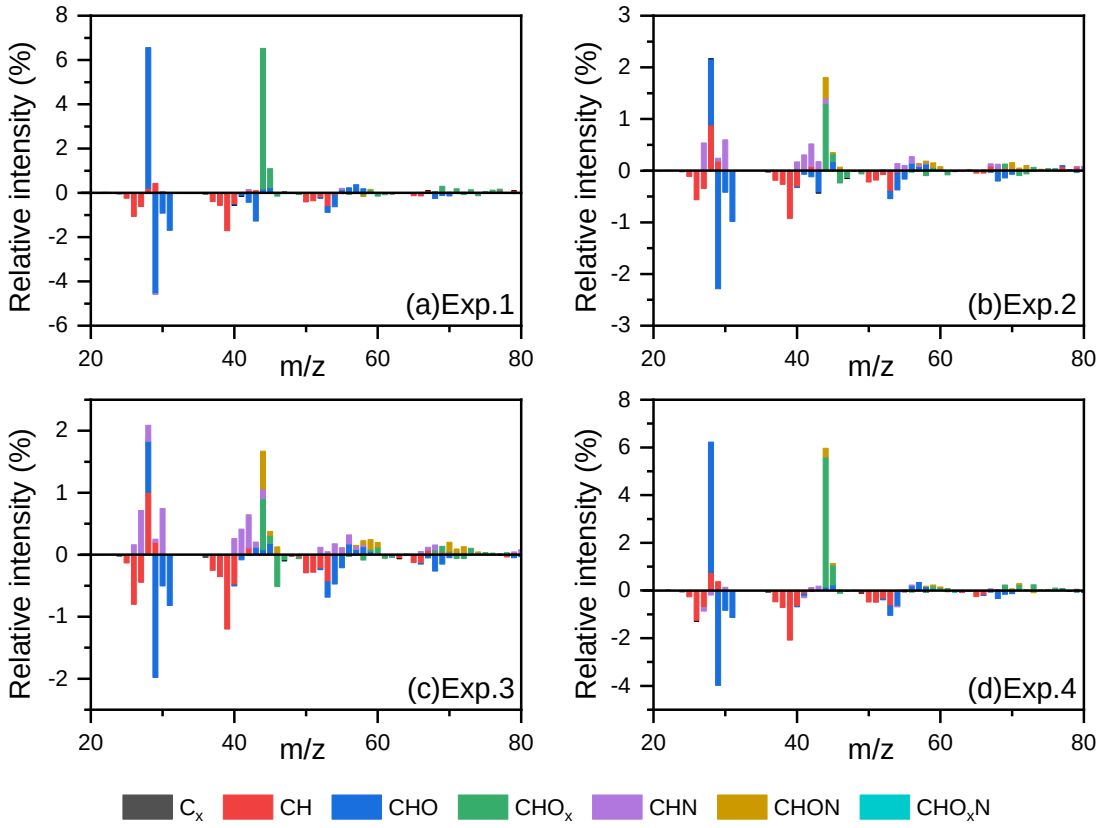

935

936 **Fig. 4.** The differential spectra of toluene SOA in the formation and stable stages. Data were taken
937 and analyzed at a high resolution but were summarized to a unit mass resolution for display. Only
938 minimal N-containing fragments could be observed in the Exp.1 without added NH_3 and NO_X.
939 These N-containing fragments could be attributed to the background NH_3 and NO_X in the chamber
940 or the systematic errors from AMS.

941

942

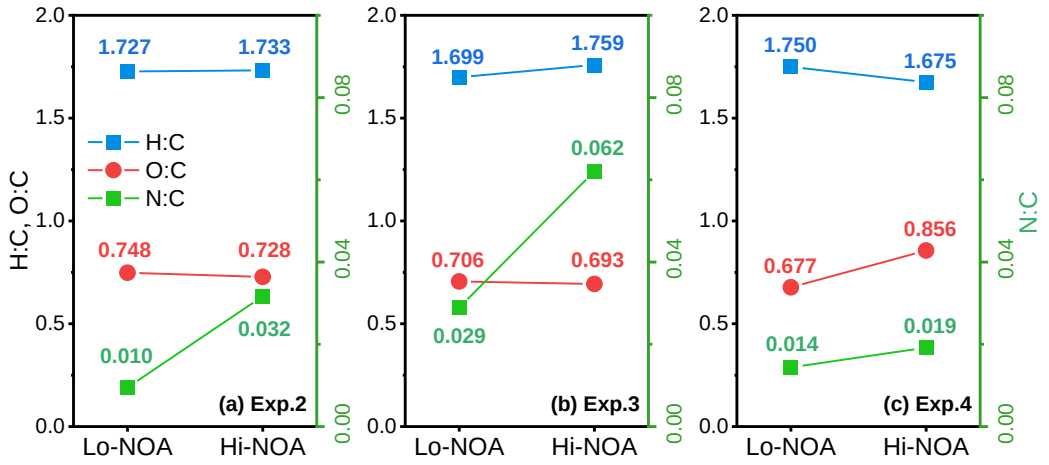

943

944 **Fig. 5.** The H/C, O/C, and N/C values of Hi-NOA and Lo-NOA for each experiment. (a) Exp. 2
945 with 200 ppb NH_3, (b) Exp. 3 with 200 ppb NH_3 and 62 ppb NO_2, and (c) Exp. 4 with 63 ppb
946 NO_2.

947

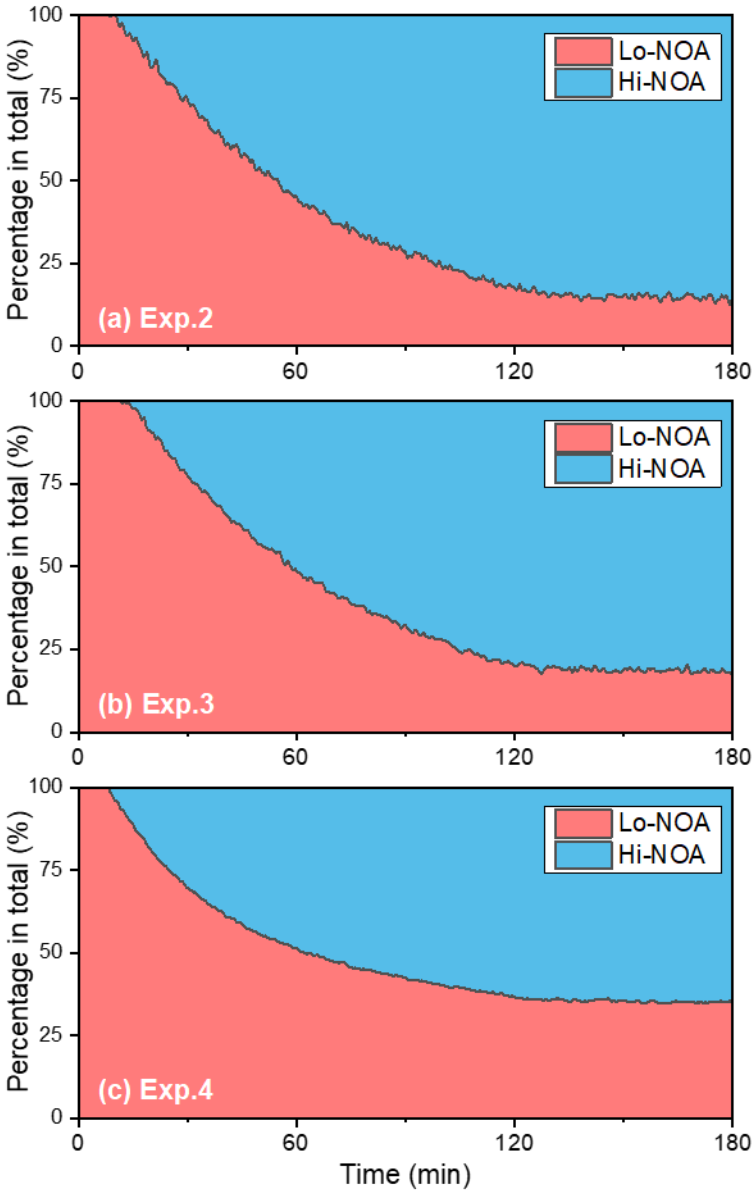

Fig. 6. The evolution of high-nitrogen OA (Hi-NOA) and low-nitrogen OA (Lo-NOA) during the photooxidation process under different NO_X/NH_3 concentrations. Hi-NOA and Lo-NOA were not consistent among experiments. (a) Exp. 2 with 200 ppb NH_3, (b) Exp. 3 with 200 ppb NH_3 and 62 ppb NO_2, and (c) Exp. 4 with 63 ppb NO_2.

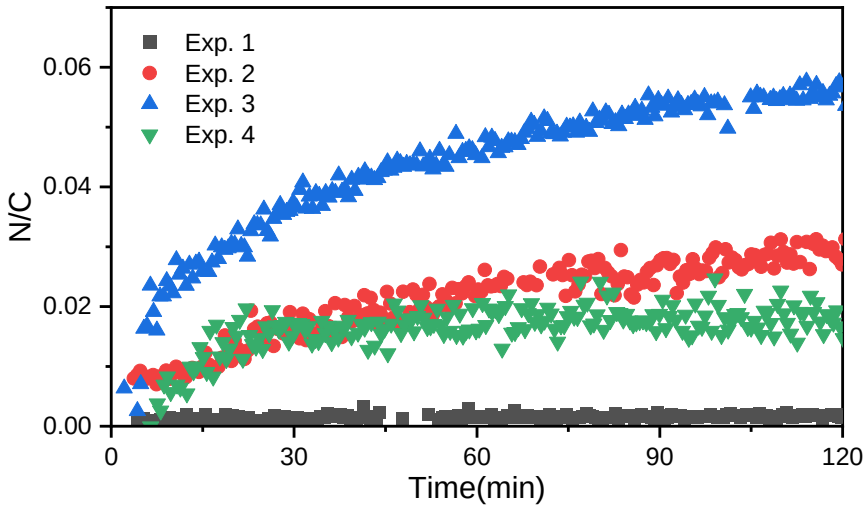

954

955 **Fig. 7.** The evolution of N/C in different experiments.

956

957

958

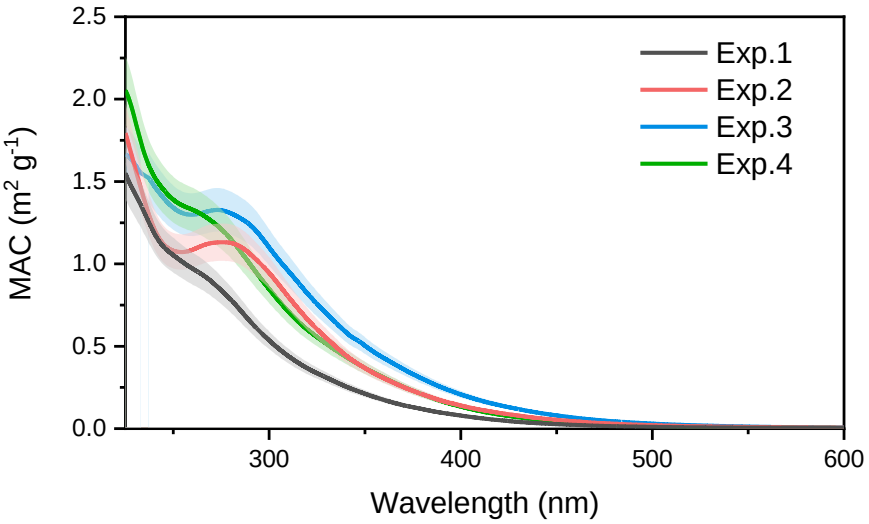

959

960 **Fig. 8.** The MAC over the range of 230 – 600 nm for the toluene SOA formed under different
961 experiment conditions.

962